Enhancing Image Quality to Improve Medical Image Classification: Application to Nuclear Medicine Planar Images

Ouassim BOUKHENNOUFA¹, Laurent COMAS^{2,3}, Jean-Marc NICOD¹, Noureddine ZERHOUNI¹, and Hatem BOULAHDOUR^{2,3}

¹SUPMICROTECH, CNRS, institut FEMTO-ST, F-25000 Besançon, France

²CHU Besançon, Médecine nucléaire, F-25000 Besançon, France ³Université de Franche-Comté, SINERGIES, F-25000 Besançon, France

Abstract

Nuclear Medicine images are obtained by injecting small amounts of radiotracers into the body to track specific organs. Particular cameras detect radiations emitted from the radio-tracers resulting in images that visualize the function of the organs rather than their structure. The association of the cameras and radiotracers causes low resolution and low signal-to-noise ratio, therefore, the images are often of poor quality. Image Quality Enhancement (IQE) is one possible solution to this problem as it improves the clarity of the images by removing noise and correcting distortions. In this paper, we propose a methodology based on artificial intelligence (AI) with the integration of an IOE step for the detection of normal/abnormal parathyroid glands. Two different IQE techniques are employed, one based on a statistical filter and the other on AI. The enhanced images are processed with a Convolutional Neural Network (CNN), and Lasso regression for features extraction and selection. Finally, several AI models are used for binary image classification. The obtained results achieved an accuracy of 83% in distinguishing normal/abnormal parathyroid glands. IQE step significantly improves the accuracy of the AI model by 16.9% over the initial accuracy of 71%, demonstrating the importance of IQE in assessing image classification performance.

Image Quality Enhancement, Artificial Intelligence, Nuclear Medicine, Medical Imaging, Parathyroid Glands.

1 INTRODUCTION

HyperParaThyroidism (HPT), is a prevalent endocrine disorder typified by elevated or anomalous parathyroid hormone levels and hypercalcemia (Walker and Silverberg, 2018). HPT can impact one or more Parathyroid Glands (PGs) (Bilezikian et al., 2016). PGs are typically 3-5 mm in size, and conventional imaging methods are unable to detect them (Sung, 2015). To give an accurate diagnosis, physicians refer to clinical data,

Nuclear Medicine (NM) images, but also other image modalities such as ultrasonography (Khan et al., 2017). There are limitations in some image modalities such as ultrasound to locate very small PGs (Lee et al., 2021).

Nuclear medicine (NM) is one remedy to this issue and improve the accuracy of physicians' diagnoses. NM is a field of medicine that uses radiopharmaceuticals to diagnose and evaluate the functioning of the body (Nieciecki et al., 2015). In NM, several image acquisition techniques exist for PGs detection in NM, double isotope and double phase are the most common. The first involves the injection of two isotopes, followed by image acquisition, while the second implicates the injection of one isotope followed by two time-domain acquisitions (Petranović Ovčariček et al., 2021). In the case of double isotope, physicians proceed with image subtraction after normalization to obtain an image with only PGs for diagnosis (Tlili et al., 2023) (Petranović Ovčariček et al., 2021).

The problem with NM images is the limitation of the information as they are very weak in signal, therefore, the images are highly noisy (Kim et al., 2020). Researchers developed different medical assistance tools based on Deep Learning (DL) to assist physicians in their diagnosis even if the related works remain limited. The study in (Yoshida et al., 2022) proposed a transfer learning methodology by applying a pretrained RetinaNet (Lin et al., 2017) model to dual-phase ^{99m}Tc-sestamibi images. The work included 281 patients with confirmed HPT, distributed as 92 for training, 45 for validation, and 44 for testing. The model achieved a sensitivity of 82% and a mean false positive indication of 0.44.

The authors in (Boukhennoufa et al., 2024) developed a medical assistance tool to automatically subtract the dual isotope ^{99m}Tc-sestamibi and ¹²³I images. The methodology consisted of combining the images with statistical features such as kurtosis and entropy extracted from each image. The images were normalized and processed with a CNN model for feature extraction, whereas the statistical features were processed with a random forest model for the same objective as with the images. The combination of the extracted features was processed with a support vector machine to predict a subtraction factor that was used to compute a subtracted image. The results yielded to a mean correlation of 0.95 with the reference images (performed by physicians).

At the preoperative level with ^{99m}Tc-sestamibi single-photon emission computed tomography, the study (Sandqvist et al., 2022) proposed to predict the presence of overlooked parathyroid hormone using six predictors such as calcium level and parathyroid hormone. The data were extracted from 349 patients with confirmed primary HPT or multi-glandular disease, and a decision tree with Bayesian hyperparameter optimization methodology was employed for the classification purpose. A 5-Fold cross-validation technique was used, where it achieved a true-positive prediction rate of 72% for multi-glandular cases and a misclassification rate of 6% for primary HPT patients.

In another study using clinical data (Samaras et al., 2024), the objective was to distinguish patients with primary HPT and Multi-Glandular Disease with an explainable machine learning methodology. The data were extracted from 134 patients and were highly imbalanced: 26 patients with MGD, and the rest with primary HPT, this issue was solved randomly by oversampling the MGD class. The used data were gender, age, size of the abnormal gland, number of affected glands, and multiplication of the parathyroid hormone with the calcium level in blood. A benchmarking of several ML algorithms such as LightGBM and support vector machine was proposed with a SHAP explainability methodology. The reported results indicated that the oversampling methodology contributed to assessing the specificity from 66.67% to 81.48%.

The different works showed promising results in HPT diagnosis using different

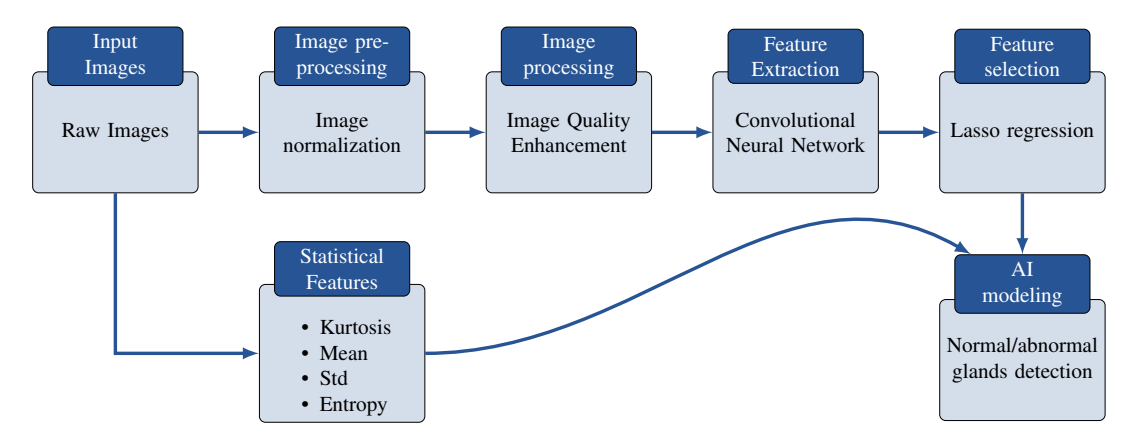


Figure 1: Overview of the proposed methodology

types of data. Nevertheless, the problem of noisy images is still not yet addressed. One remedy is to apply Image Quality Enhancement (IQE): an important step to improve the precision of DL models. IQE consists of removing noise and improving the brightness of images to highlight important features (Bhardwaj et al., 2018). To the best of our knowledge, there is no other study including an IQE step for PGs detection.

In this paper, we propose a new process for normal/abnormal PGs detection by applying two IQE techniques on only dual-isotope static images. The first employs a statistical filter approach, while the second is based on AI. The filtered images are passed into a DL model and a Lasso regression for feature extraction and selection. Finally, AI models are benchmarked for image classification.

The remainder of the paper is organized as follows: Section 2 details the used data and the proposed methodology. Section 3 presents and discusses the results of the proposed approach. The work is concluded in Section 4.

2 MATERIALS AND METHODS

In this section, the patient's demographics, the used data, and the proposed methodology are explained.

2.1 Patients and data characteristics

Between June 2012 and December 2023, 923 patients underwent dual isotope (99mTc-sestamibi/¹²³I) planar scintigraphy. The acquisitions were realized on a Discovery NMCT 670 or an Infina GE Healthcare. First, 18.5 MBq +-10% of ¹²³I was administered intravenously. 3h later, 740 MBq +/- 10% of ^{99m}Tc-sestamibi was injected. 5 min later, the acquisition started with planar imaging of the thyroid region (PINHOLE) for 10 min and mediastinum Low Energy High Resolution (LEHR) for 5 min (dual isotope setting with photopeak's centered over 140,5 keV +/-7,5% and 159 keV -5% + 10% window for ^{99m}Tc-sestamibi and ¹²³I, respectively). A subtraction of the two PINHOLE images is performed using XELERIS Software by the physicians. They begin by extracting the thyroid from the ¹²³I image, which is merged with the ^{99m}Tc-sestamibi image. Next, the images are normalized according to the thyroid intensity in both images. This ensures that both images are uniformly scaled. The subtraction

is performed and adjusted then between the two normalized images (Tlili et al., 2023). This results in a Subtracted Image (SI), used by the physicians to identify abnormal PGs

Due to the absence of images in the Picture Archive and Communication Systems, scintigraphy with no thyroid fixation in some cases, and cases judged doubtful case by physicians, 215 patients were removed. The characteristics are summarized in Table 1. In this study, 5 images per patient are used: LEHR of 99m Tc-sestamibi and 123 I, PINHOLE of 99m Tc-sestamibi and 123 I, and the Subtracted Image. The image size is 128×128 pixels with a grayscale channel.

Table 1: Patient's characteristics summary

Patients	Age	Gender	Weight	Height
number	range	F:M	range	range
708	[18 - 99]	601:222	[40 - 167]	[143 - 189]

2.2 Proposed methodology

Figure 1 highlights the overall process of the proposed methodology, starting with raw images as inputs to the AI modeling where the objective is to detect abnormal PGs.

From raw images, statistical features are extracted and are used later in the process: kurtosis, mean pixel value, standard deviation, and entropy. The objective of these features is to help the AI model in PGs diagnosis. These characteristics can help the model understand extracting patterns between images of normal/abnormal PGs cases. For instance, in the images of abnormal glands, the mean pixel value may be larger than in normal glands. Also, since the quantity of used data is not very high, adding these features means adding more data, hence, enlarging the population. The next step of the methodology consists of image normalization, as explained in Subsection 2.1, the normalization performed by physicians is one important step in order to subtract the images. Also, in the AI pipeline, image normalization is a very important step to increase performance and speed up the learning convergence. For these reasons, the images in this study are normalized using the MinMax normalization method (Zhang et al., 2024). Specifically, each image type is normalized globally, meaning that the images are scaled in function of the minimum and maximum pixel values of the whole dataset. For example, in LEHR ^{99m}Tc-sestamibi of each patient, the images are normalized with the minimum and maximum pixel values of all the LEHR 99mTc-sestamibi images. This ensures that the images are normalized uniformly and the characteristics of all the data are taken into account. Equation 1 represents the normalization, where NI, RI, t, n represents Normalized Image, Raw Image, one of the image types, and the number of patients, respectively.

$$NI_{MinMax} = \frac{RI_t - \min(RI_1, ...RI_n)}{\max(RI_1, ...RI_n) - \min(RI_1, ...RI_n)}$$
(1)

The second step of the process is about enhancing the quality of images, once the images are normalized, they're processed with two different techniques and compared differently according to the diagnosis results. The first is based on a statistical filter called Non-Local Means Denoising (NLMD) (Buades et al., 2011). The latter is an image processing technique for IQE, it reduces the noise by averaging similar pixels throughout the whole image. In opposition to other statistical filters that consider only neighborhood pixels, NLMD locates patches of pixels with similar patterns across all

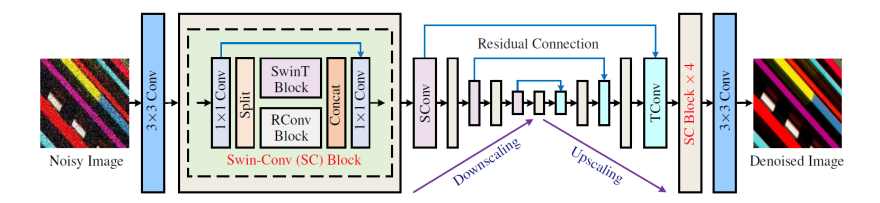


Figure 2: SCUNet architecture from (Zhang et al., 2023). Licensed under a Creative Commons Attribution 4.0 International License (CC BY 4.0). No modifications were made

the images. These patterns are used to remove noise more effectively, but also preserve the details of the images. NLMD is a form of segmentation as it merges the pixels with similar characteristics into patches. NLMD computes the denoised pixel value by using a weighted average of all the image pixels as shown in Equation 2. Where i and j are positions of the pixel values. \hat{P}, P are the denoised pixel value at position i, original pixel value at position j, respectively. w is the similarity weight between pixels at position i and j. Finally, C represents a normalization factor ensuring that weight sum to 1 shown in Equation3.

$$\hat{P}(i) = \frac{1}{C(i)} \sum_{j} w(i,j) P(j)$$
(2)

The weights are computed with an Euclidean distance as represented in Equation 3, where I(i) and I(j) are patches centered around i and j. A filtering parameter h is used to control the degree of smoothing, defined as 0.8 in this study.

$$w(i,j) = e^{-\frac{\|I(i)-I(j)\|^2}{h^2}}, C(i) = \sum_{j} w(i,j)$$
(3)

NLMD ensures that pixels similar to one in the position *i* contribute more to its denoising value, reducing noise while preserving important details. For all these reasons, NLMD is chosen in this work. The second IQE technique is based on AI using a Swin-Conv-UNet (SCUNet) denoising network. It is a combination of Swin transformers, Convolution Neural Network (CNN), and U-NET model. A Swin-Conv (SC) block is used as the main backbone of the U-NET model (Zhang et al., 2023). SCUNet performs in a segmentation way where it groups patches of similar patterns. To the best of our knowledge, it is the state-of-the-art image denoising model. For these reasons, it is used in this study to provide a fair comparison with NLMD as they both perform with the patch principle. Figure 2 details the architecture of the SCUNet model. The images are first passed to a convolution filter of size 3, followed by the SC block, the U-NET model with residual connections, and finally, another SC block and a convolution filter of size 3 to reconstruct the denoised image.

The IQE methodologies are summarized in Figure 3 where IQE1 and IQE2 represent the NLMD and SCUNet techniques, respectively. The two IQEs are used separately for the five different images (PINHOLES ^{99m}Tc-sestamibi, ¹²³I, and subtracted), (LEHR ^{99m}Tc-sestamibi and ¹²³I).

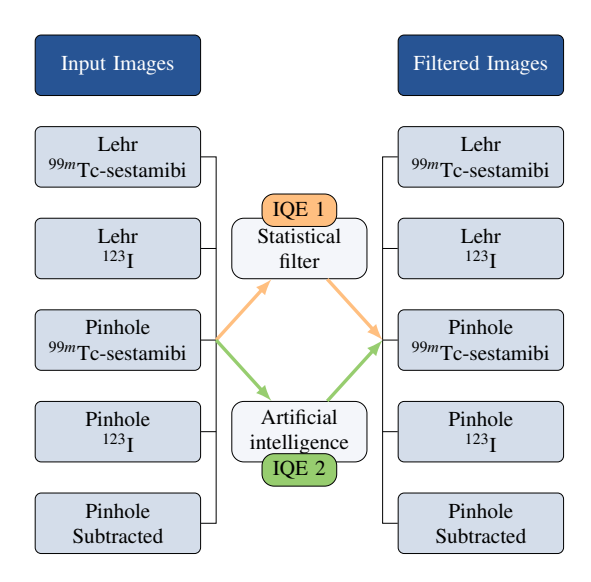


Figure 3: Image Quality Enhancement process

In the third step of the process and once the images are processed for IQE, a CNN is used for feature extraction, to decrease the size of the images and preserve only the important features for further processing. After a series of trials, the architecture in Table 2 was found to be the best performing one for the diagnosis purpose. The input layer is of shape $128 \times 128 \times 1 = 16384$ features.

Table 2: CNN architecture for feature extraction

Layer	Hyperparameters
Conv2D	- 32 filters of size 3,
	relu function
MaxPooling2D	- filter size of 2
Conv2D	- 64 filters of size 3,
	relu function
Batch Normalization	/
MaxPooling2D	- filter size of 2
Conv2D	- 128 filters of size 3,
	relu function
MaxPooling2D	- filter size of 2
GlobalAveragePooling2D	/
Dense	128 nodes, relu function

The fourth step of the methodology consists of applying the Least Absolute Shrinkage and Selection Operator (Lasso) regression (Tibshirani, 1996) for feature selection before feeding them to AI models for classification. Lasso is a form of linear regression that aims to reduce and remove non-relevant/redundant features to avoid over-fitting. This is achieved by shrinking some features to zero, leaving only the most important ones. Lasso prevents over-fitting problems and can do both feature selection and regularization, which leads to more generalized models. A pair of features with corresponding labels (0 for normal glands and 1 for abnormal). The objective is to minimize the

function represented in Equation (4). y is the label, X are the features, β a coefficient for each feature, n the number of patients, f the total number of features.

minimize
$$\left(\sum_{k=1}^{n} \left(y_i - \sum_{z=1}^{f} X_{kz} \beta_j\right)^2 + \lambda \sum_{z=1}^{f} |\beta_z|\right)$$
(4)

Lasso is a modified version of linear regression by the addition of the penalty term $\lambda \sum_{z=1}^{f} |\beta_z|$ that helps the model in the generalization process and avoids over-fitting.

The last step of the process consists of concatenating the statistical features extracted at the beginning from the raw images and the features resulting from the Lasso regression into a single matrix that is used for binary classification. The latter is achieved by benchmarking several Machine Learning (ML) algorithms. The training is consolidated with a 10-Fold cross-validation technique. The data are divided into 10 folds, for 10 iterations, 9 folds are used for the model training and 1 fold for validation. This ensures that all the data are used at least one time for training and once for testing, it also reduces the variance in the performance providing trustful results, more reliable model evaluation, and a robust model.

With this proposed methodology, it is ensured that only important features from the enhanced images are used with an addition of the statistical information to enrich the training of the ML models with the objective of improving the diagnosis. Also, the quantity of data is not very high, for these reasons, the choice of ML models for image classification is evident.

3 RESULTS AND DISCUSSIONS

In this section, the results of the proposed methodologies are detailed with discussions.

3.1 Image quality enhancement

In order to evaluate the IQE techniques, the two most common metrics for such tasks are employed: Peak Signal-to-Noise Ratio (PSNR), and Structural Similarity Index Measure(SSIM). Both metrics are used to evaluate the image-denoising, PSNR measures the quality of a denoised/reconstructed image compared to the original. A value higher than 30dB indicates a high image quality enhancement, whereas a lower value expresses a lower IQE. SSIM measures the similarity between two images by comparing the luminance, contrast, and structure. Its values range between [0-1], from poor quality to very high quality.

Table 3 shows the obtained results applying the two metrics on the used data, the values are the mean across the whole data with the 5 different image types.

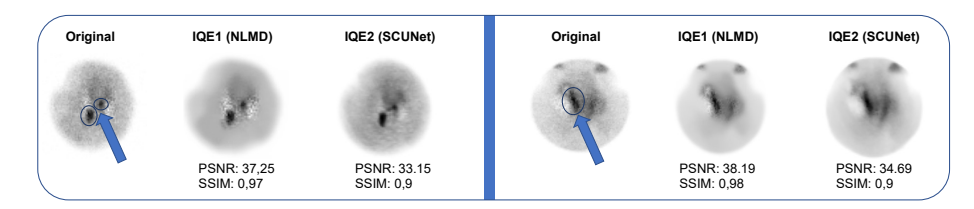


Figure 4: Example application of NLMD and SCUNet on subtracted PINHOLE

Table 3: Performance evaluation of IQE techniques. P: PINHOLE, L: LEHR

Image type	IQE technique	PSNR	SSIM
D 99mm1.	IQE1	38.54	0.98
P. ^{99m} Tc-sestamibi	IQE2	32.65	0.91
P 123I	IQE1	37.46	0.97
P1	IQE2	31.52	0.79
Subtracted P.	IQE1	37.85	0.97
Subtracted P.	IQE2	32.42	0.85
L. ^{99m} Tc-sestamibi	IQE1	39.44	0.98
L. 1C-sestamoi	IQE2	33.47	0.92
I. 123 I	IQE1	39.52	0.98
L1	IQE2	30.65	0.75

The results report a dominance using IQE1 (statistical filter-based method), in comparison to IQE2 (AI-based method). The filter-based methodologies are simpler and designed especially for special tasks, image denoising in this context, making them highly effective for IQE purposes. Another reason is that filters apply a fixed set of operations and treat the images individually according to their local characteristics which leads to reliable results. On the other hand, AI-based methodologies for IQE are more complex and require a large amount of data, which leads to the non-generalization of new data. Finally, the dataset is very limited in terms of size which led to the SCUNet model not performing well compared to NLMD. AI-based techniques may capture information that isn't caught by traditional filters, but for this specific task in this work, NLMD is more performant as the goal is to enhance the image quality, while features (information) are extracted later in the process.

An example application of the two IQEs (NLMD and SCUNet) on two random subtracted PINHOLES of two patients is shown in Figure 4. NLMD effectively reduces the noise and enhances the key regions (indicated in circles) with arrows in the original images while maintaining the important structures such as the edges of the images, also in terms of metrics it achieved PSNR of 37.25, and 38.19, respectively in the two cases. On the other hand, the application of the SCUNet (IQE2) filter in the same two cases reports a decrease in the PSNR and SSIM with 4.1 and 0.07, respectively. It results in partial noise removal without completely reducing it. Important structures, such as edges, were slightly modified, resulting in a loss of information that could affect the performance of ML models in terms of accurate image classification.

In summary, with IQE1 the noise is removed from images without modifying the structures which is the objective of the use case in this study. NLMD (IQE1) is selected over SCUNet (IQE2) for the next steps and the rest of the process.

3.2 Image classification

The images are processed with IQE1, and fed to the CNN for feature extraction and Lasso regression for feature selection. A benchmarking of ML models for binary classification (normal/abnormal PGs detection) is applied. The images are associated with the extracted statistical features explained in Subsection 2.2. The corresponding labels are divided into 472 positive (abnormal), and 236 negative (normal). The imbalanced data problem is solved by reducing the number of positive cases to 250. As a result, 250 positive and 236 negative cases are used to benchmark the ML models. The remaining positive cases aren't discarded as they're used in the test phase.

Table 4 reports the results with different ML models with various metrics: Accuracy, Area Under Curve, and Recall. The best-performing model is presented in each image type with the mean values reported by 10-Fold cross-validation. The results clearly show that PINHOLE images outperform LEHR images. This was expected since physicians primarily rely on the PINHOLE images for the diagnosis.

Table 4: Classification results with IQE1. P: PINHOLE, L: LEHR

Image type				
P. ^{99m} Tc-sestamibi	LGBM	77%	74%	73%
P. ¹²³ I	RF	75%	71%	71%
Subtracted P.	LGBM	81%	80%	80%
L. ^{99m} Tc-sestamibi	SVM	67%	66%	67%
L. ¹²³ I	SVM	65%	65%	63%
Combined P.	LGBM	83%	83%	81%

The combination of the 3 PINHOLE images improves the performance by 2.47%. This suggests that using multiple images provides integral information, which increases the model's ability to make more accurate classifications.

To study the ability of the model to distinguish between the normal and abnormal classes, an AUC metric was used that gave different results in Table 4. A Receiver Operating Characteristic (ROC) curve with the combination of the 3 PINHOLE images using LGBM is presented in Figure 5. The corresponding AUC is 0.83 (83%) which expresses a good-performing model indicating the high ability to differentiate between the two classes, meaning that the model does not tend to a particular class.

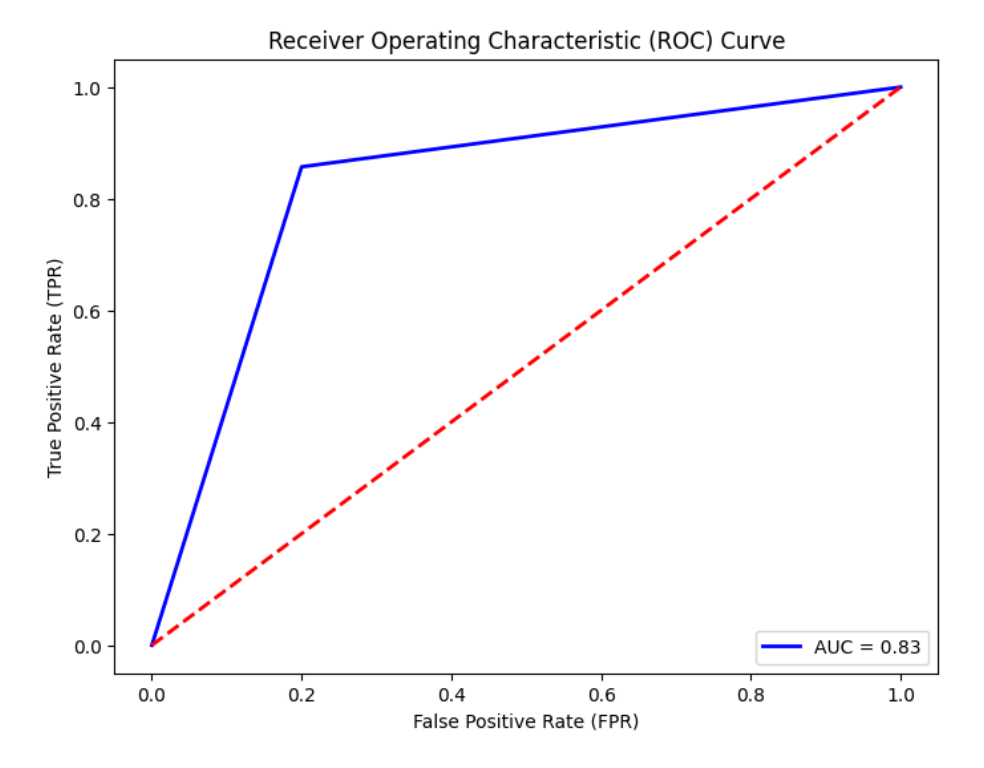


Figure 5: ROC curve with the test data

The results are good, but there is still room for improvement. A perfect AUC should be 1.0 (100%), further future works needs to be oriented in a way to improve this value by increasing the size of the dataset if available, or AI model improvement.

3.3 Ablation study

To study the impact of IQE1 on image classification with the different ML models, an ablation study is performed. To achieve this, the proposed approach was repeated without the image processing (IQE1) step. The aim is to evaluate the contribution of IQE1 to the global methodology, and whether the performance increases or not. The obtained results as highlighted in Table 5 show a significant decrease in the performance, for example, using combined PINHOLES, the accuracy dropped by 14.4% compared to the methodology with IQE1 application. This significant decrease in accuracy emphasizes the important role of IQE1 in assessing image classification performance. IQE1 improves image quality by removing noise and highlighting darker regions, this improves the relevance and details of images. By doing so, the ML models focus more on the key features in the images, resulting in improved performance.

Table 5: Classification results with IQE1. P: PINHOLE, L: LEHR

Image type	Model	Acc	AUC	Recall
P. ^{99m} Tc-sestamibi	LGBM	67%	63%	62%
P. ¹²³ I	RF	69%	69%	68%
Subtracted P.	LGBM	70%	69%	69%
L. ^{99m} Tc-sestamibi	SVM	58%	57%	58%
L. ¹²³ I	SVM	61%	62%	63%
Combined P.	LGBM	71%	70	70%

This study clearly demonstrates that IQE1 is crucial to ensuring that AI models achieve optimal performance by providing cleaner, more targeted input images.

3.4 Performance limitations

As mentioned in Section 1, physicians usually rely on multiple data sources before giving the final diagnosis. The proposed methodology demonstrates good performance even when relying on a single type of data (static images). This highlights the effectiveness of the proposed approach in providing reliable insights with limited data, especially in scenarios where access to multiple modalities is limited.

While the proposed methodology achieves an accuracy of 83%, the remaining 17% represents cases where the model couldn't give the real class label (as given and assigned by senior physicians). Figure 6 shows an example of misclassification, the predicted labels are in red, whereas the real labels are below each case. For the right case, the affected PG can't be observed in the image as it is in the posterior of the thyroid, only its corresponding tomographic images could reveal the PG. On the other hand, in the right case, the image reveals a gland in the blue circle, however, the diagnosis report revealed that it was a thyroid gland and not a PG. The computed tomography images were able to show this difference.

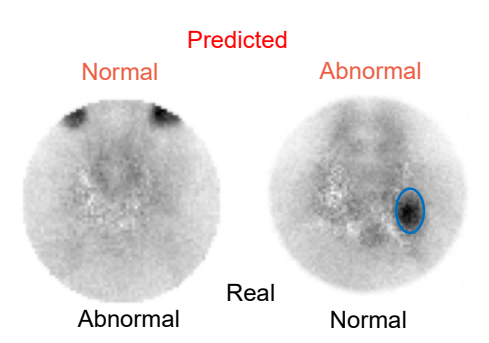


Figure 6: Misclassification example

For future works, including tomographic images should be considered for an accurate diagnosis, as it proved its efficiency (Öksüz et al., 2011) (Petranović Ovčariček et al., 2021). Also, medical object detection and segmentation could be more accurate as they only focus on specific regions of images.

4 CONCLUSIONS

This paper presented a methodology for abnormal PGs detection using static dualisotope ^{99m}Tc-sestamibi and ¹²³I PINHOLE and LEHR images. First, statistical features were extracted to be combined with the images for classification. The images were normalized using the MinMax technique. Then, an image processing approach for IQE was applied using the statistical filter-based technique IQE1 (NLMD) and AI-based approach IQE2 (SCUNet). The obtained results showed that IQE1 outperformed IQE2 for this task, therefore IQE1 was selected for the rest of the process. Next, the filtered images were fed to CNN for feature extraction and then to Lasso for feature selection. Finally, the statistical features were combined with the selected features for normal/abnormal PGs diagnosis. After extensive simulations, the results showed that the proposed methodology achieved an accuracy of 83% by combining the PINHOLE images. The results also showed that IQE1 improved the diagnosis results by 16.9%, boosting image classification. The obtained performance indicates the potential of the proposed methodology to be a reliable medical assistance tool by providing a primary diagnosis using only one type of data.

COMPLIANCE WITH ETHICAL STANDARDS

This study was registered by the Clinical Research and Innovation Delegation of the University Hospital Center of Besancon under the number 2023/796.

ACKNOWLEDGMENT

This work has been achieved in the frame of the EIPHI Graduate school (contract "ANR-17-EURE-0002").

REFERENCES

- Bhardwaj, N., Kaur, G., and Singh, P. K. (2018). A systematic review on image enhancement techniques. *Sensors and Image Processing: Proceedings of CSI 2015*, pages 227–235.
- Bilezikian, J., Cusano, N., Khan, A., Liu, J., Marcocci, C., and Bandeira, F. (2016). Primary hyperparathyroidism. nature reviews disease primers. 2016; 2: 16033.
- Boukhennoufa, O., Comas, L., Nicod, J.-M., Ungureanu, C., Zerhouni, N., and Boulahdour, H. (2024). Automatic detection of parathyroid glands in nuclear medicine. In 2024 IEEE International Symposium on Biomedical Imaging (ISBI), pages 1–4. IEEE.
- Buades, A., Coll, B., and Morel, J.-M. (2011). Non-local means denoising. *Image Processing On Line*, 1:208–212.
- Khan, A., Hanley, D., Rizzoli, R., Bollerslev, J., Young, J., Rejnmark, L., Thakker, R., D'amour, P., Paul, T., Van Uum, S., et al. (2017). Primary hyperparathyroidism: review and recommendations on evaluation, diagnosis, and management. a canadian and international consensus. *Osteoporosis International*, 28:1–19.
- Kim, K., Lee, M.-H., and Lee, Y. (2020). Investigation of a blind-deconvolution framework after noise reduction using a gamma camera in nuclear medicine imaging. *Nuclear Engineering and Technology*, 52(11):2594–2600.
- Lee, S.-W., Shim, S. R., Jeong, S. Y., and Kim, S.-J. (2021). Direct comparison of preoperative imaging modalities for localization of primary hyperparathyroidism: a systematic review

- and network meta-analysis. JAMA Otolaryngology–Head & Neck Surgery, 147(8):692–706
- Lin, T.-Y., Goyal, P., Girshick, R., He, K., and Dollár, P. (2017). Focal loss for dense object detection. In *Proceedings of the IEEE international conference on computer vision*, pages 2980–2988.
- Nieciecki, M., Cacko, M., and Królicki, L. (2015). The role of ultrasound and nuclear medicine methods in the preoperative diagnostics of primary hyperparathyroidism. *Journal of Ultrasonography*, 15(63):398–409.
- Öksüz, M. Ö., Dittmann, H., Wicke, C., Müssig, K., Bares, R., Pfannenberg, C., and Eschmann, S. M. (2011). Accuracy of parathyroid imaging: a comparison of planar scintigraphy, spect, spect-ct, and c-11 methionine pet for the detection of parathyroid adenomas and glandular hyperplasia. *DIR*, 17(4):297.
- Petranović Ovčariček, P., Giovanella, L., Carrió Gasset, I., Hindié, E., Huellner, M. W., Luster, M., Piccardo, A., Weber, T., Talbot, J.-N., and Verburg, F. A. (2021). The eanm practice guidelines for parathyroid imaging. *EJNMMI*, 48:2801–2822.
- Samaras, A.-D., Tsimara, M., Voidila, S., Papandrianos, N., Zampakis, P., Moustakidis, S., Papageorgiou, E., and Kalogeropoulou, C. (2024). Explainable classification of patients with primary hyperparathyroidism using highly imbalanced clinical data derived from imaging and biochemical procedures. AS, 14(5):2171.
- Sandqvist, P., Sundin, A., Nilsson, I.-L., Grybäck, P., and Sanchez-Crespo, A. (2022). Primary hyperparathyroidism, a machine learning approach to identify multiglandular disease in patients with a single adenoma found at preoperative sestamibi-spect/ct. *European Journal* of Endocrinology, 187(2):257–263.
- Sung, J. Y. (2015). Parathyroid ultrasonography: the evolving role of the radiologist. *Ultra-sonography*, 34(4):268.
- Tibshirani, R. (1996). Regression shrinkage and selection via the lasso. *Journal of the Royal Statistical Society Series B: Statistical Methodology*, 58(1):267–288.
- Tlili, G., Mesguich, C., Gaye, D., Tabarin, A., Haissaguerre, M., and Hindié, E. (2023). Dual-tracer 99mtc-sestamibi/123i imaging in primary hyperparathyroidism. *QJNMMI*.
- Walker, M. D. and Silverberg, S. J. (2018). Primary hyperparathyroidism. *Nature Reviews Endocrinology*, 14(2):115–125.
- Yoshida, A., Ueda, D., Higashiyama, S., Katayama, Y., Matsumoto, T., Yamanaga, T., Miki, Y., and Kawabe, J. (2022). Deep learning-based detection of parathyroid adenoma by 99mtc-mibi scintigraphy in patients with primary hyperparathyroidism. *Annals of Nuclear Medicine*, 36(5):468–478.
- Zhang, K., Li, Y., Liang, J., Cao, J., Zhang, Y., Tang, H., Fan, D.-P., Timofte, R., and Gool, L. V. (2023). Practical blind image denoising via swin-conv-unet and data synthesis. *Machine Intelligence Research*, 20(6):822–836.
- Zhang, Z., Zhang, Q., Gao, Z., Zhang, R., Shutova, E., Zhou, S., and Zhang, S. (2024). Gradient-based parameter selection for efficient fine-tuning. In *Proceedings of the IEEE/CVF Conference on Computer Vision and Pattern Recognition*, pages 28566–28577.